

Analytical simulation of reversed cyclic lateral behaviors of an RC shear wall sub-assembly

Han Seon Lee*, Da Hun Jeong and Kyung Ran Hwang

*School of Civil, Environmental, and Architectural Engineering, Korea University,
74 Incheon-ro, Sungbuk-gu, Seoul, 136-713, Korea*

(Received July 26, 2011, Revised January 9, 2012, Accepted February 2, 2012)

Abstract. Experimental results of cyclic reversed lateral force test on a two-story reinforced concrete shear wall sub-assembly are simulated analytically by using the PERFORM-3D program. A comparison of experimental and analytical results leads to the following conclusions: (1) “Shear Wall” and “General Wall” models with “Concrete shear” cannot simulate the pinching phenomena due to shear and show larger amounts of inelastic energy absorption than those in the experiment. (2) Modeling a story-height wall by using two or more “General Wall” elements with “Diagonal shear” in the vertical direction induces the phenomenon of swelling-out at the belly, leading to the erroneous simulation of shear behaviors. In application to tall building structures, it is recommended to use one element of “General Wall” with “Diagonal shear” for the full height of a story. (3) In the plastic hinge area, concrete deformations of analytical models overestimate elongation and underestimate shortening when compared with experimental results.

Keywords: reinforced concrete; nonlinear analysis; PERFORM-3D; wall sub-assembly.

1. Introduction

More than 58% of the total number of housing units, approximately over 10 millions, use apartment buildings as dwelling houses in Korea (KNSO 2010). These residential apartment buildings generally consist of high-rise reinforced concrete (RC) wall structures. The style of these RC structures such as shown in Fig. 1(a) is unique around the world and the seismic performance of these structures has been investigated with due interest, neither in Korea nor abroad. The available approach to observe the seismic response of these structures subjected to strong earthquake ground excitations is to use the nonlinear history analyses or to conduct earthquake simulation tests on the small-scale models. Even with the test conducted, the adopted models are usually restricted to simple or reduced-scale models due to limitations of the capacity of available laboratories. These limitations of earthquake simulation tests render the analytical prediction of seismic responses a viable alternative. However, it is important to balance model simplicity with the ability to reliably predict the inelastic response both at the global and local levels under seismic loads to ensure that the analytical model captures the hysteretic wall behavior and the interaction between the wall and other structural members and the foundation reasonably well (Wallace 2007). Analysis programs that are available to practicing engineers to predict the nonlinear behavior of large scale RC

* Corresponding author, Professor, E-mail: hslee@korea.ac.kr

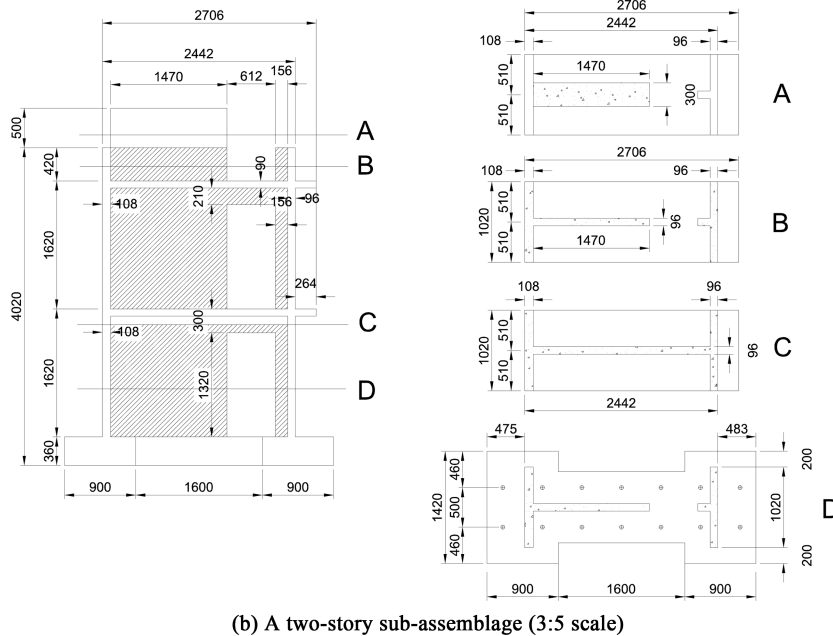
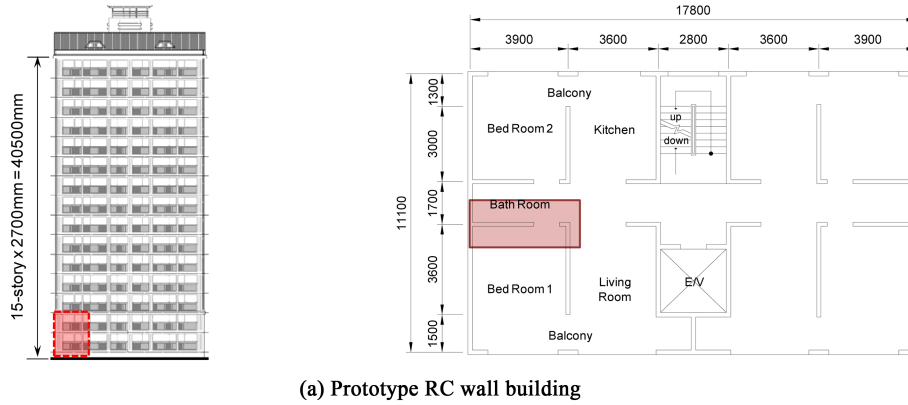


Fig. 1 Elevation and plan of prototype RC wall building and a two-story sub-assembly (unit: mm)

structures are very scarce. Martinelli and Fillippou (2009) used OPENSEES (McKenna and Fenves 2006) to simulate the seismic response of 7-story full-scale wall structures. Mo *et al.* (2008) also used this program to predict the behavior of RC wall-type structures under cyclic loading. And Kwak and Kim (2004) presented a numerical model in finite element analysis to simulate the nonlinear response of RC shear walls under reversed cyclic loading. Orakcal and Wallace (2006) adopted the MVLEM model to simulate the static test results of wall specimens with high accuracy. However, these softwares are research-oriented and not tailored for the practicing engineers to apply to real building structures. Schotanus and Maffei (2009) used commercial softwares, ETABS (CSI 2006) and PERFORM-3D (CSI 2006), to calibrate the stiffness of RC members and to analyze the contribution of wall and slabs using the 7-story benchmark experiment (Panagiotou *et al.* 2006).

Recently, performance-based seismic engineering (PBSE) including the assessment of existing

structures and the design of new structures has become a standard procedure in some leading design offices. Typical standard guides regarding the PBSE are the FEMA 356 (FEMA 2000) and the ASCE/SEI 41 (ASCE 2007) reports. With this trend, the use of reliable nonlinear analysis softwares is crucial to successful PBSE. Despite the sophisticated accuracy of softwares used within the research group, practicing engineers are not able to apply these softwares to practice due to the following facts: (1) The capacity of research-oriented softwares is generally limited to analysis of elements or small-size structures, and usually does not include pre- and post-processors for assessment and design. In other words, these research-oriented softwares are not suitable to be used for real large-scale building structures. (2) The uncertainties regarding the information of existing and new structures do not warrant the complicated specific modeling as performed by researchers in nonlinear analysis of elements and structures. And (3) the time and effort required for practicing engineers to perform analysis with a high level of accuracy is not generally warranted within the budget of the project. Therefore, practicing engineers compromise and resort to commercially-developed softwares.

One of the commercial softwares most widely used around the world is PERFORM-3D. This program focuses on PBSE with the incorporation of the analytical models provided in the FEMA 356 (FEMA 2000), ASCE-SEI 41(ASCE 2007) and PEER/ATC-72-1(PEER/ATC 2010) guidelines. However, as cited in the PERFORM-3D manual, the wall models of this program have not been calibrated for any experimental results. Although Powell, the developer of this program, in the personal communication with the first author (Powell 2011), insists that: “its purpose is to calculate deformation and strength demands, and hence demand/capacity ratios, which can be used to make decisions for practical design. It is not intended for general purpose nonlinear analysis, where the goal is “exact” simulation of actual behavior - that is, given the geometry of a structure and its (nonlinear) material properties, calculate (simulate) the “exact” behavior of the structure,” it is clear that most of the users want to know how well PERFORM-3D can simulate the real behavior of structures and how the model parameters affect the analytical results. The aims of the research stated herein are to calibrate analytical models available in PERFORM-3D, through comparing the analytical results with the experimental obtained through reversed cyclic lateral force tests on a two-story reinforced concrete wall sub-assembly and, thereby, to provide useful information in the establishment of the models and the interpretation of the analysis results.

2. Outline of experiment

The prototype for the experiment was determined to represent the most typical design in Korea. The floor area of one family unit is 89 m² and one story accommodates two family units, while the number of stories is 15 as shown in Fig. 1(a). The design was performed according to the old Korean building code (AIK 2000). The thickness of walls is generally 200 mm or less with the two layers of vertical (longitudinal) and horizontal (transverses) reinforcements. Reinforcements in walls are *D16*, *D13* and *D10* with *D16* and *D13* used for vertical, or longitudinal, reinforcements. *D10* is usually used for the horizontal, or transverse, reinforcement of walls and the slab. Details of transverse reinforcements are nonseismic and do not comply with the requirement of the special walls in ACI 318-02 (ACI 2002).

A two-story sub-assembly was extracted from this prototype as shown in the shaded area in Fig. 1(a). Considering the capacity and space of the available laboratory at Busan National University,

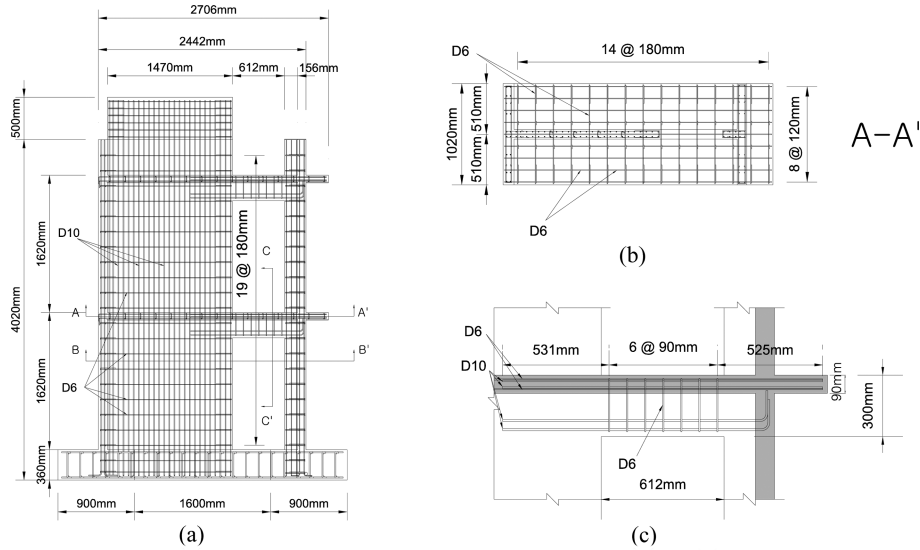


Fig. 2 Dimensions and details of 3:5 scale specimen: (a) Elevation, (b) Plan of slab and (c) Detail of coupling beam (See Fig. 17 for *B-B'* section and Fig. 16(a) for *C-C'* section)

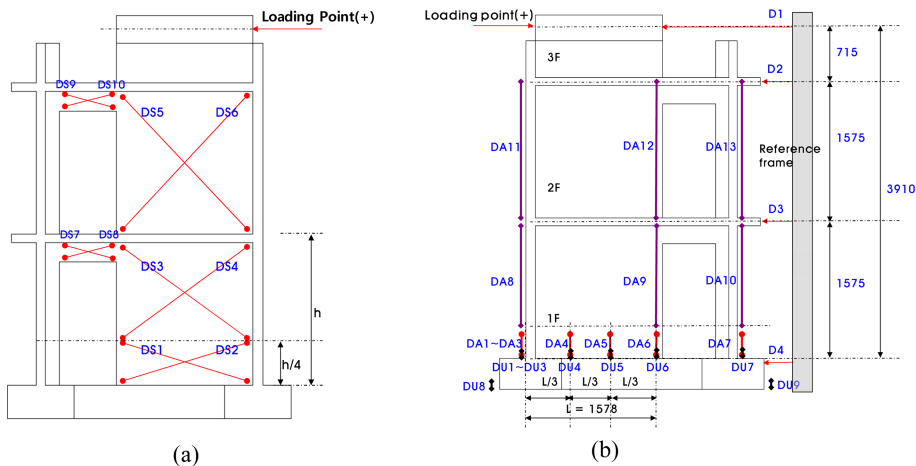


Fig. 3 Instrumentations (unit:mm): (a) Shear deformation and (b) Lateral story displacement and axial and rotational deformation

Korea, the specimen was reduced to a 3:5 scale as shown in Fig. 1(b). Although this subassembly was extracted from the bottom part of the 15-story building structure, the gravity axial force was not applied due to the limitation in the capacity of the laboratory. Details of this specimen are given in Fig. 2. The steel ratio of the longitudinal reinforcement in the main web wall is 2.78% with that of the transverse bars being 0.327%. *D10* and *D6* were used in the 3:5 scale specimen to represent *D16* and *D10* in the prototype. *D19* was used for the foundation of the specimen to increase its rigidity and strength. The *D10* and *D6* used have the yield strengths of 567 MPa and 364 MPa, respectively, with the tensile strength of 638 MPa and 583 MPa, and the elongations of 7% and 6%, respectively. The compressive strength of concrete was 23.9 MPa with the design strength of 24

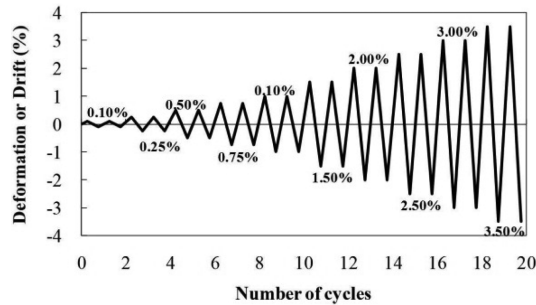


Fig. 4 Loading protocol (unit: %)

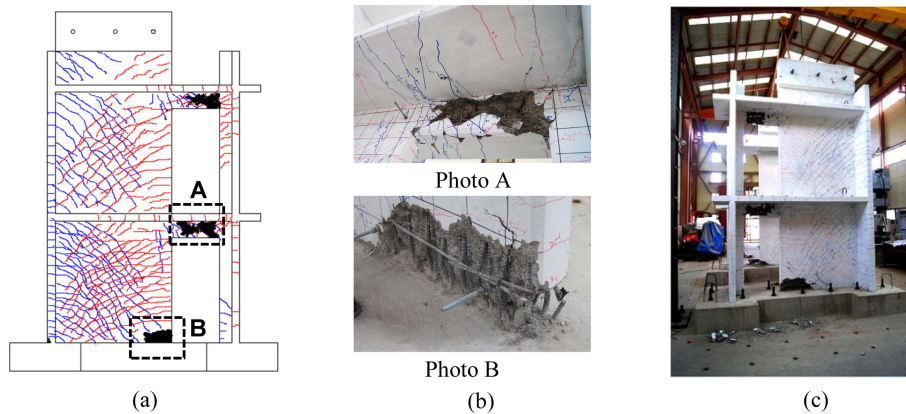


Fig. 5 Crack and damage patterns of the specimen: (a) Cracks and damages, (b) Enlarged photos and (c) Overall view of damaged specimen

MPa. In Fig. 3, instrumentations were established to measure four lateral story displacements ($D1\sim D4$), nine vertical deformations ($DA1\sim DA9$), nine uplift deformations ($DU1\sim DU9$), ten shear deformations ($DS1\sim DS10$), and the lateral force and displacement of the actuator. The experiment was performed following the lateral displacement protocol in Fig. 4.

Fig. 5 shows crack and damage patterns of the specimen after the completion of the experiment. The main failure mode in damage and crack patterns appeared to be the combined flexural and shear failure. Detailed descriptions of crack and damage developments are given in Table 1 for each critical drift ratio. The specimen revealed the maximum resistance, 538 kN at the drift ratio of 1.44% in the positive direction while it showed the maximum resistance 497 kN at the drift ratio of 1.43% in the negative. After these peak resistances, the specimen showed the tensile opening failure at the joint between the foundation and the flange wall, the compressive concrete crushing at the edge of the web wall beside the bottom of the opening at the first story and at the coupling beams, which led to the sudden drop in the resistance and finally to the buckling and fracture of the reinforcement. Detailed information on these experiments is given in Lee *et al.* (2010).

Table 1 Development of cracks and damage

Drift ratio	0.1%	0.25%	0.5%	0.75%
Left flange wall	Initiation of flexural crack in the 1st story wall	Increase of the number of cracks in the 1st story wall	Increase of number of cracks in the 1st and 2nd story walls.	Initiation of up-lift at bottom
Web wall	Initiation of flexural and shear crack in the 1st story wall	Initiation of crack in the 2nd story wall	Initiation of concrete spalling at the bottom near opening	Increase of concrete spalling at the bottom near opening
Coupling beam	Initiation of shear crack in the 1st and 2nd story beams	Increase of the number of cracks	Increase of crack width	Increase of crack width
Right flange wall	No crack	Initiation of flexural crack	Initiation of vertical crack	Increase of crack width
Slab	Initiation of flexural cracks at the boundaries between coupling beam and web walls	Increase of the number of cracks	Increase of crack width	Increase of crack width
Drift ratio	1.0%	1.5%	2.0%	
Left flange wall	Increase of crack width	Concentrated increase of up-lift at bottom	Concentrated increase of up-lift at bottom	
Web wall	Spalling of concrete at the bottom near opening	Buckling of longitudinal bar at bottom near opening	Fracture of longitudinal bar at bottom near opening	
Coupling beam	Initiation of concrete spalling in the 1st story coupling beam	Spalling of concrete in the 1st, 2nd story coupling beams	Spalling of concrete in the 1st, 2nd story coupling beams	
Right flange wall	Increase of crack width	Increase of crack width	Increase of crack width	
Slab	Increase of crack width	Penetration of cracks through the slab thickness	Concentrated increase of crack width above the coupling beam	

3. Analytical modeling

3.1 Concepts of wall models in PERFORM-3D

There are two types of wall elements, “Shear Wall” and “General Wall” in PERFORM-3D. This section is a reduced reproduction from “elements and component of PERFORM-3D” (CSI 2006) regarding wall elements to assist with the presentation and interpretation of the correlation between analysis and test results. However, since this section is not considered to represent fully the intention of the manual of PERFORM-3D, direct reference to this manual is recommended.

3.1.1 Shear Wall

The following are some key points of shear wall elements:

- (1) Each element connects 4 nodes and has 24 degrees of freedom.
 - (2) Longitudinal (usually vertical) in-plane behavior is more important than transverse (usually horizontal) behavior. In the longitudinal direction the element can be inelastic in bending and/or shear. Transverse in-plane bending is also secondary, and is assumed to be elastic.
 - (3) For the purposes of calculating the element stiffness, the cross section depth is assumed to be constant along the element length, based on the element width at its mid-height.
 - (4) As the fibers yield and/or crack in an inelastic fiber section, the effective centroidal axis shifts. However, the axial extension of an element is always calculated at the midpoint of the cross section (i.e., the longitudinal axis of the element does not shift).
 - (5) Axial strain, shear strain and curvature are assumed to be constant along the element length. Hence, a “Shear Wall” element is a lower order element than a typical beam element, where the curvature varies linearly. With a single element to model a one-story wall, from beam theory the calculated elastic bending deflection is only 75% of the “exact” deflection. This is a concern only for a wall with one or two stories. For taller walls it is sufficiently accurate to use one element per story.
- A “Shear Wall” element has no in-plane rotational stiffness at its nodes. To specify a moment-resisting connection between a beam and a wall, a beam element should be imbedded in the wall.

3.1.2 General Wall

The “General Wall” element is an “engineering” element intended for the specific purpose of modeling a wall. It is not a general purpose finite element. To model bending, shear and diagonal compression behavior, an example element consists of five layers, acting in parallel as shown in Fig. 6. The layers are as follows:

- (1) Axial-bending layer for the vertical axis, as shown in Fig. 6(a). The cross section is a fiber section with steel and concrete fibers. This allows the neutral axis to shift as the concrete cracks.
- (2) Axial-bending layer for the horizontal axis, as shown in Fig. 6(b). This is also a fiber section.
- (3) “Concrete shear layer”, as shown in Fig. 6(c). This assumes constant shear stress and a uniform wall thickness. The shear properties for this layer are based on the contribution of the concrete to the shear strength, and it will be termed the “concrete shear”, or “concrete shear” layer.
- (4) “Diagonal compression layer” for downwards diagonal, as shown in Fig. 6(d). This assumes

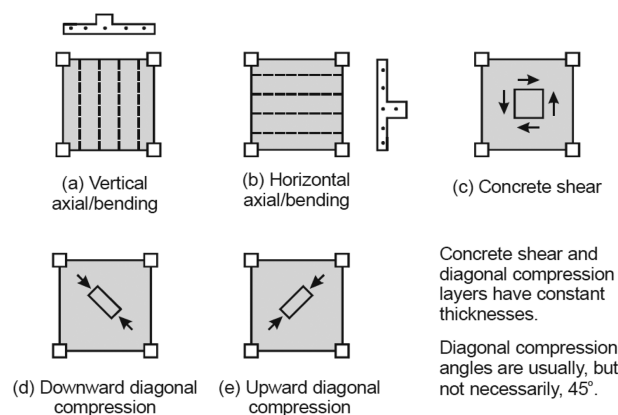


Fig. 6 Representable behaviors of the “General Wall” element (Courtesy of CSI)

constant diagonal compression stress and a uniform wall thickness. The slope of the diagonal wall is usually, but not necessarily, 45 degrees. Through interaction with the axial-bending layer, this layer transmits shear and accounts for the contribution of the reinforcing steel to the shear strength. The mechanism is explained later. This is a “Diagonal shear layer”.

(5) “Diagonal compression layer” for upward diagonal, as shown in Fig. 6(e). Each layer shows different behavior. The layers interact because they are connected at the nodes. The combined behavior of all layers defines the behavior of the element.

If the two “Diagonal layers” are neglected, the “General Wall” element is similar to the “Shear Wall” element, in which the major difference is that fiber sections are used for both horizontal and vertical cross sections. Therefore, unless diagonal strut action is important for the structure and the structure is dealt with the added complexity, it is suggested that the diagonal layer be ignored in PERFORM-3D. The original statement of this paragraph in the manual is emphasized in bold face as follows: “Unless you believe that diagonal strut action is important for your structure, and you are prepared to deal with the added complexity, we suggest that you ignore the diagonal layers”.

In the actual wall the concrete is in a state of multi-axial stress. For example, there could be combined vertical compression, horizontal tension and shear. The inelastic behavior of a material under multi-axial stress is much more complex than its behavior under uniaxial stress. This is especially true for concrete. The General Wall element does not consider multi-axial stress. Instead it separates the various aspects of behavior into layer, with uniaxial stress in each layer. Some consequences of this are as follows:

(1) The axial-bending layers account for vertical and horizontal compression stresses in the concrete, and the diagonal layers account for diagonal compression stresses. In an actual wall these stresses interact directly. For example, instead of crushing vertically under a large vertical stress, the presence of a diagonal stress might cause the concrete to crush along an inclined direction, at a lower vertical stress than if the diagonal stress were not present. This type of effect is not considered in the element. The axial-bending layers interact with the diagonal layers, because they are connected at the element nodes, but this interaction is not the same as the interaction associated with multi-axial stresses.

(2) When concrete is subjected to combined compression and shear, the shear strength is increased, essentially because there is internal friction. The “General Wall” element does not account for frictional behavior. The shear strength in the “Concrete shear layer” is assumed to be independent of any other stresses.

Fig. 7 shows the shear stress and the equivalent diagonal stresses for the concrete shear case; Shear stress on the horizontal and vertical edges corresponds to equal tension and compression stresses along the diagonals. Fig. 8 shows similar diagonal for the diagonal compression case. In

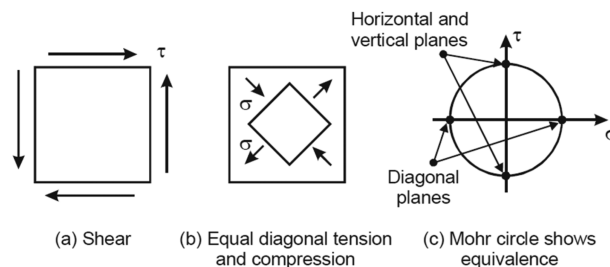


Fig. 7 Equivalent stresses for concrete shear (Courtesy of CSI)

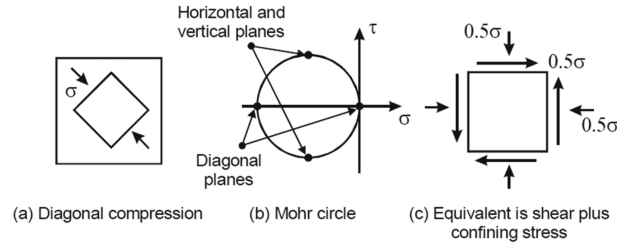


Fig. 8 Equivalent stresses for diagonal compression (Courtesy of CSI)

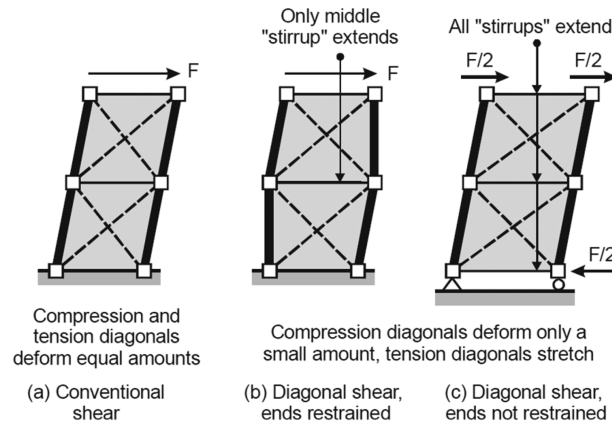


Fig. 9 Shear deformations (Courtesy of CSI)

this case, a diagonal compression stress of σ is equivalent to a shear stress of 0.5σ plus horizontal and vertical compression (confining) stresses of 0.5σ . A key point for the diagonal compression case is that unless the confining stress is present there can be no diagonal compression stress (i.e., if the confining stress, 0.5σ , is zero, the diagonal compression stress, σ , must also be zero). In a reinforced concrete web it must be provided by horizontal steel reinforcement (shear stirrups) in the web. In effect, horizontal tension in these stirrups provides horizontal confining compression in the concrete, which is then able to resist diagonal compression stresses.

Fig. 9 shows the example cantilever with shear deformations and negligible bending. Fig. 9(a) shows the case with only concrete shear. This case assumes that the web material has diagonal tension strength as well as compression strength, and that there are equal and opposite strains in the compression and tension diagonals. Horizontal stirrups are not needed, and if such stirrups are present they do not have tension forces. In the “General Wall” element, the “Concrete shear layer” provides shear behavior of this type. Figs. 9(b) and (c) show the case with only diagonal compression. In this case the tension diagonals crack. There must be horizontal stirrups, and there are tension forces in these stirrups. The stirrups will usually be flexible relative to the compression diagonals, so most of the effective shear deformation is due to stretching of the stirrups rather than compression of the diagonals. Fig. 9(b) shows the case where the end cross sections are restrained, and only the center stirrup deforms. Fig. 9(c) shows the case where the end cross sections are not restrained, and all of the stirrups deform. In this case the effective shear deformation is larger. In the “General Wall” element, the “Diagonal compression layers, interacting with the horizontal axial/bending layer, provide shear behavior of this type.

The axial/bending layers account for bending behavior. These layers consist of steel and concrete fibers. The edges of the element are constrained to remain straight, which means that plane sections remain plane within a single element. An important aspect of bending behavior in reinforced concrete is that as the concrete cracks and the steel yields, the neutral axis shift. Hence, bending and axial effects are coupled, with the following effects:

- (1) If the neutral axis shifts, a bending moment causes not only curvature but also axial extension.
- (2) If there is an axial compression force on a cross section, the bending strength is increased, because cracking of the concrete is delayed.

The “General Wall” element uses fiber cross section components to model the axial/bending behavior. A fiber cross section captures the above interaction effects.

Fig. 10 shows two ways in which there can be extension of the axial/bending layer. Fig. 10(a) shows simple vertical extension, and Fig. 10(b) shows bending along the vertical axis. If the neutral axis shifts, as will usually be the case, bending causes axial extension. Fig. 10(c) shows Mohr’s circle for strain for the case in Fig. 10(a). For 45 degree diagonals an axial tension strain of ϵ , causes tension strains of 0.5ϵ along each diagonal direction. Since diagonal compression materials have no tension strength, the diagonals crack and the diagonal stresses are zero. The situation is the same for axial extension that is caused by bending and shift of the neutral axis. Within a single “General Wall” element the diagonal strains depend on the vertical strain at the axis of the axial/bending layer. Consider an element that has no “Concrete shear layer”, so that shear is carried only by the “Diagonal compression layer”. If shear is added to Fig. 10(b), the “Diagonal compression layer” will offer no shear resistance until one of the diagonals goes into compression. This means that if the axial strain is ϵ , a shear strain equal to ϵ must be added before there is any shear resistance. Mohr’s circle for strain at this point is shown in Fig. 11.

The physical significance for reinforced concrete is shown in Fig. 12. As shown in Fig. 12(a), the

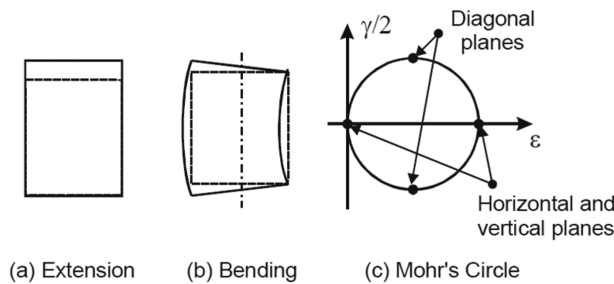


Fig. 10 Effect of vertical extension on diagonal strain (Courtesy of CSI)

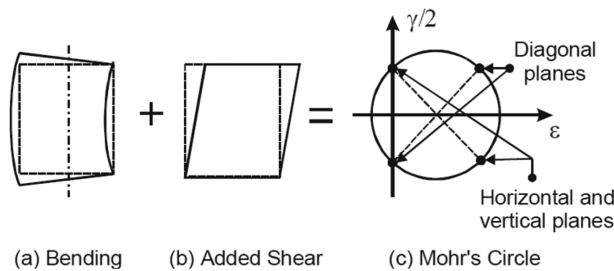


Fig. 11 Mohr’s circle when diagonal gap closes (Courtesy of CSI)

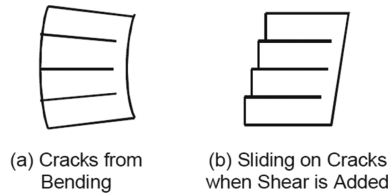


Fig. 12 Behavior in reinforced concrete (Courtesy of CSI)

bending deformation causes cracking of the concrete. As shown in Fig. 12(b), when the shear deformation is added there must be shear sliding displacements across the cracks. A real concrete beam would provide resistance to these displacements by a variety of mechanisms. In a “General Wall” element this type of resistance is modeled by the “Concrete shear layer”. A “General Wall” with both “Concrete shear” and “Diagonal compression layer” would predict resistance based on the “Concrete shear layer” alone until the gaps close in the “Diagonal compression layer”, then resistance from both layers.

3.2 Modeling of a 2-story wall sub-assembly

Relationships between stress and strain for reinforcements and concrete are given in Figs. 13(a) to (c). Most of the transverse reinforcements correspond to non-seismic details. So, the concrete is assumed to be unconfined. The tensile strength of concrete was assumed to be negligible. Also, the compressive strain of reinforcements at the buckling is assumed to be 0.01 m/m, and the

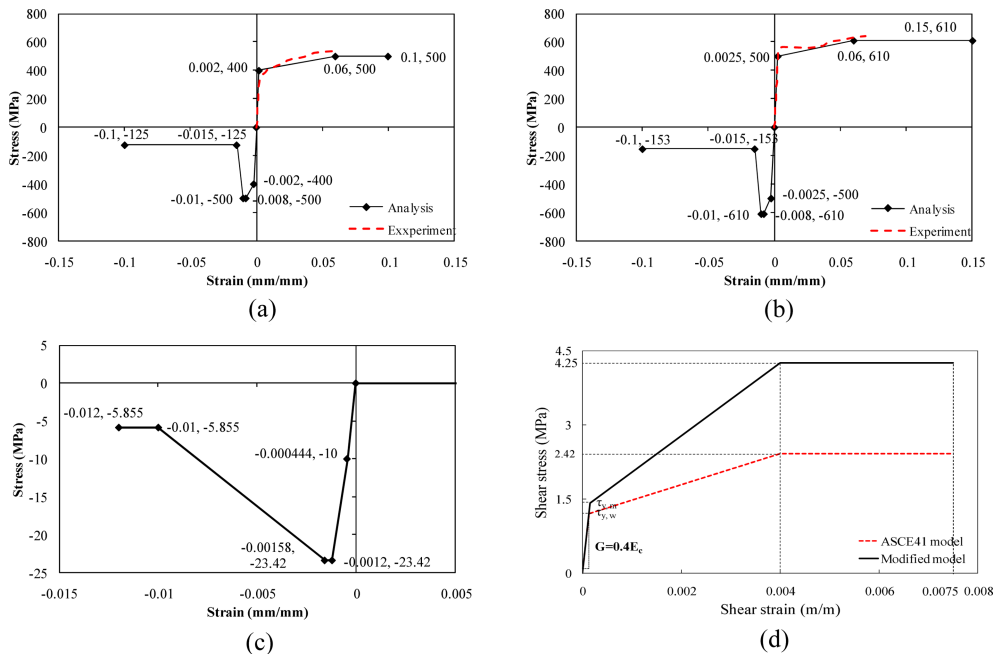


Fig. 13 Stress-strain relation of material: (a) Steel D6 ($E = 200,000$ MPa), (b) Steel D10 ($E=200,000$ MPa), (c) Concrete ($E = 22,540$ MPa) and (d) Inelastic shear material for a wall ($G = 9,020$ MPa)

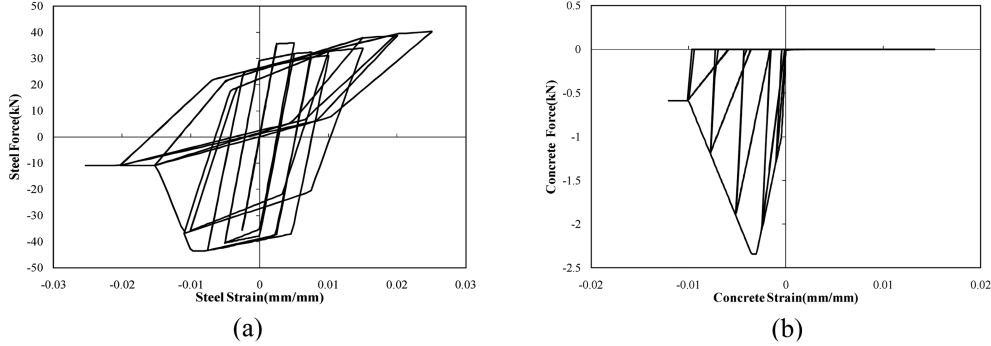


Fig. 14 Hysteretic behavior of steel and concrete fiber subjected to axial loading protocol in Fig. 4: (a) Steel model (D10) and (b) Concrete model

compression strain of concrete at the strength degradation is assumed to start at 0.00158. Cyclic behaviors of reinforcements and concrete are given in Figs. 14(a) and (b).

Hognestad model was adopted for the concrete. However, because the envelope curve provided in PERFORM-3D cannot accept this model directly, the segmentally-linear model was used to describe this model. Although Hognestad model with the monotonic loading has the ultimate strength strain $\varepsilon_0 = 1.8 f'_c / E_c = 0.00187$ m/m ($f'_c = 23.4$ MPa, $E_c = 22,540$ MPa), the yield strain of 0.00158 m/m was used based on the empirical judgment to account for the softening due to the tensile cracking before compression. As already explained in the description of damage and crack development, since the drift ratio of 1.4% at the loading point induced the maximum resistance and the compressive crushing of concrete, followed by the buckling of the vertical longitudinal reinforcement, it seems to be reasonable to assume the maximum strain in compressive yielding of reinforcement, 0.01 m/m, because PERFORM-3D does not have any model for buckling of reinforcement.

The backbone relation between shear strain and shear stress for the concrete shear is given in Fig. 13(d). The shear backbone curve obtained using Eq. (1) according to ASCE/SEI 41 is denoted by dotted lines and the adjusted curve to fit the experimental results is shown with solid lines

$$v_n = \alpha_s \sqrt{f'_c} + \rho_t f_y = 2.42 \text{ MPa} \quad (1)$$

where

v_n = Shear strength, $\alpha_s = 0.25$, $f'_c = 24$ MPa (Concrete compressive strength),

$\rho_t = 0.00327$ (ratio of horizontal reinforcement), $f_y = 364$ MPa (yield strength of D6)

The initial shear modulus is assumed to be $0.4E_c = 9,020$ MPa with a yield strain of 0.004 m/m, where E_c is modulus of elasticity of concrete. The material properties of “diagonal compression layer” were assumed to be identical to the concrete material. The physical calibration was conducted by adjusting the thickness of this layer.

The first series of mesh models is established as follows: Model S1 has one Wall element in each story, and Model S2 and Model S3 have two “Shear Wall” elements in the first story with different locations of division, a half point in Model S2 and a lower quarter point in Model S3. Models, G1, G2 and G3, have the same mesh models as Models, S1, S2 and S3, respectively, but use “General Wall” elements with the “Concrete shear” instead of the “diagonal compression layer” (Figs. 15(a) to (c)). It is possible to use the “General Wall” element which combines the shear models of “Concrete shear” and “diagonal compression layer” by adjusting the thickness of wall assigned to

each shear model. In this study, the “General Wall” element with 100% of “Concrete shear” (100% of the thickness is assigned to “Concrete shear”), 100% of “Diagonal compression layer” (100% of the thickness is assigned to “Diagonal shear”), and 50% of concrete shear” with 50% of “Diagonal shear” will be attempted. FEMA 356 recommends that the hinge length of wall is the lower of half of the wall length and the story height. Models *S2* and *G2* represent this recommendation. Models *S3* and *G3* are devised to simulate the local behaviors as obtained from the instrumentation in Fig. 3, by which the distributions of concrete strains in the lower quarter region and the rotation and shear deformations of the upper and lower parts in the first story were measured. Unfortunately, since the data of rotation obtained from the lower quarter part were not reliable, the data of rotation and shear obtained from the upper part are used to compare with analytical results.

The second series of mesh models, Model *G1* to Model *G5*, are established using “General Wall” elements with “Diagonal compression layer” only. Compared to Model *G3*, Model *G4* has three wall elements in the horizontal direction in the main web wall, while Model *G5* has the additional horizontal division at the vertical half point, and it therefore results in a finer mesh as shown in Figs. 15(d) and (e). All the mesh models include the slab and coupling beam in Fig. 16(a). However, this slab model is formulated for visual purposes only by reducing the effective thickness to 1 mm. Instead, the slabs were modeled as beams imbedded in shear walls. Models *G1* through *G5* use the beam elements to describe the behavior of coupling beams in Fig. 16(a). However, *G6* replaces this beam model by “General Wall” in Fig. 15(f).

The ends of the coupling beams are modeled as a “Moment Hinge” of the “Rotation Type”, while the center is modeled with a “Shear Hinge” of the “Rigid-Plastic Strain Type” as shown in Fig. 16(b). The yield moment and yield shear force in the coupling beam are given in Fig. 16(a). Because the length of the coupling beam is short, the coupling beam is expected to yield in shear before yielding in flexure. Therefore, the “Shear Hinge” is located at the center of the beam, while

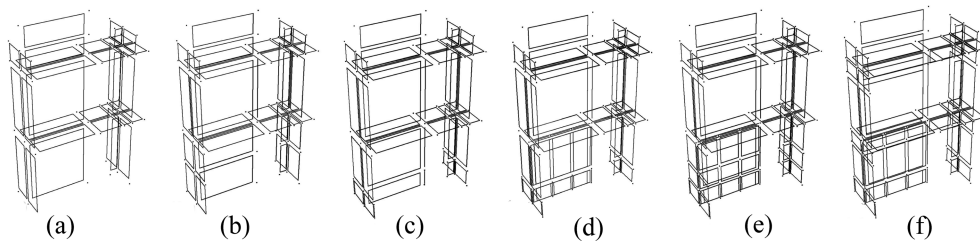


Fig. 15 Analytical mesh models: (a) Model *S1/G1*, (b) Model *S2/G2*, (c) Model *S3/G3*, (d) Model *G4*, (e) Model *G5* and (f) Model *G6*

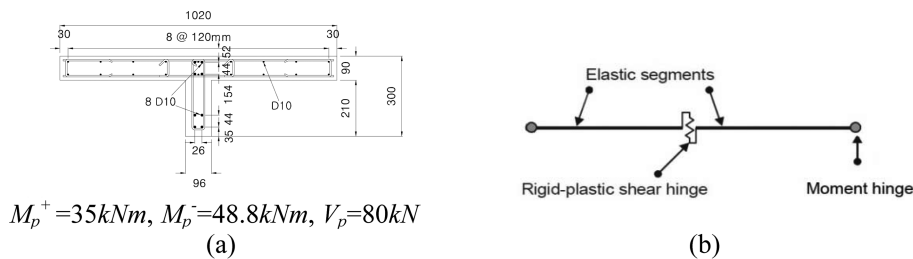


Fig. 16 Modeling of coupling beam (Models *G1* to *G5*, Models *S1* to *S3*): (a) Section of coupling beam (unit: mm) and (b) Coupling beam “Component” (Courtesy of CSI)

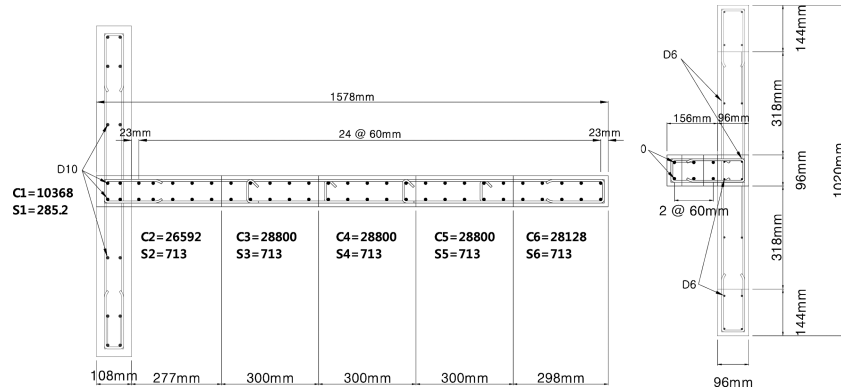


Fig. 17 Example of fibers in a web wall of Model S1/G1 (unit: mm, mm²) (C1 to C6: concrete fibers, S1 to S6: steel fibers)

the “Moment Hinge” is adopted at both ends of the coupling beams to accommodate the flexural yielding at these locations. The shear force by the yield moment is estimated to be ($V_{mp} = (M_p^+ + M_p^-)/l = (35 \text{ kNm} + 48.8 \text{ kNm})/0.612 \text{ m} = 137 \text{ kN}$). The yield shear strength (V_p) is assumed to be the sum of the yield strength (V_s) by shear reinforcements and shear strength (V_c) contributed by concrete ($V_p = V_s + V_c = 80 \text{ kN}$). The horizontal section of the web wall is divided for models S1 and G1 by several concrete and reinforcement “Fibers” as shown in Fig. 17.

4. Correlation of experiment and analysis

4.1 Global behaviors

The relations between the lateral force and lateral displacement at the top of the models for Models S1 to S3, and G1 to G3 are compared with the experimental result shown in Fig. 18. It should be noted that Models, S1, S2 and S3 use the vertical axial/bending layer and the “Concrete shear layer” while Models, G1, G2 and G3 adopt both vertical and horizontal axial/bending layers, with the same “Concrete shear layer”. In Fig. 18, behaviors of the Model G series and the Model S series are similar in strength and stiffness. When the analytical results obtained by using Models S1, S2 and S3 are compared, it is noted that the two-element models (Models S2, S3) reveal lower strengths closer to the test results than one-element model (Model S1).

The same trend can be found in the results of Models, G1, G2 and G3. However, all the analytical curves obtained from the models shown in Fig. 18 show similar initial stiffness, but larger energy absorption than the experimental curves. Considering the cyclic degradation of shear materials, the energy factors of Shear material 1 were assumed to be “1, 0.3, 0.25, 0.2, 0.1”, and the energy factors of Shear material 2 were assumed to be “1, 0.85, 0.7, 0.4, 0.3” for Model G3. Although the hysteretic shear behaviors of these two shear materials reveal relatively large difference in local behaviors in Fig. 22(b), global behaviors are similar in Fig. 18(f). Global behaviors are little affected by energy factors of shear material.

The hysteretic relations between the lateral force and displacement at the top of the specimen are given in Fig. 19 for Models G1 to G5 (“General Wall”) as defined in Fig. 15. In Fig. 19(a), the

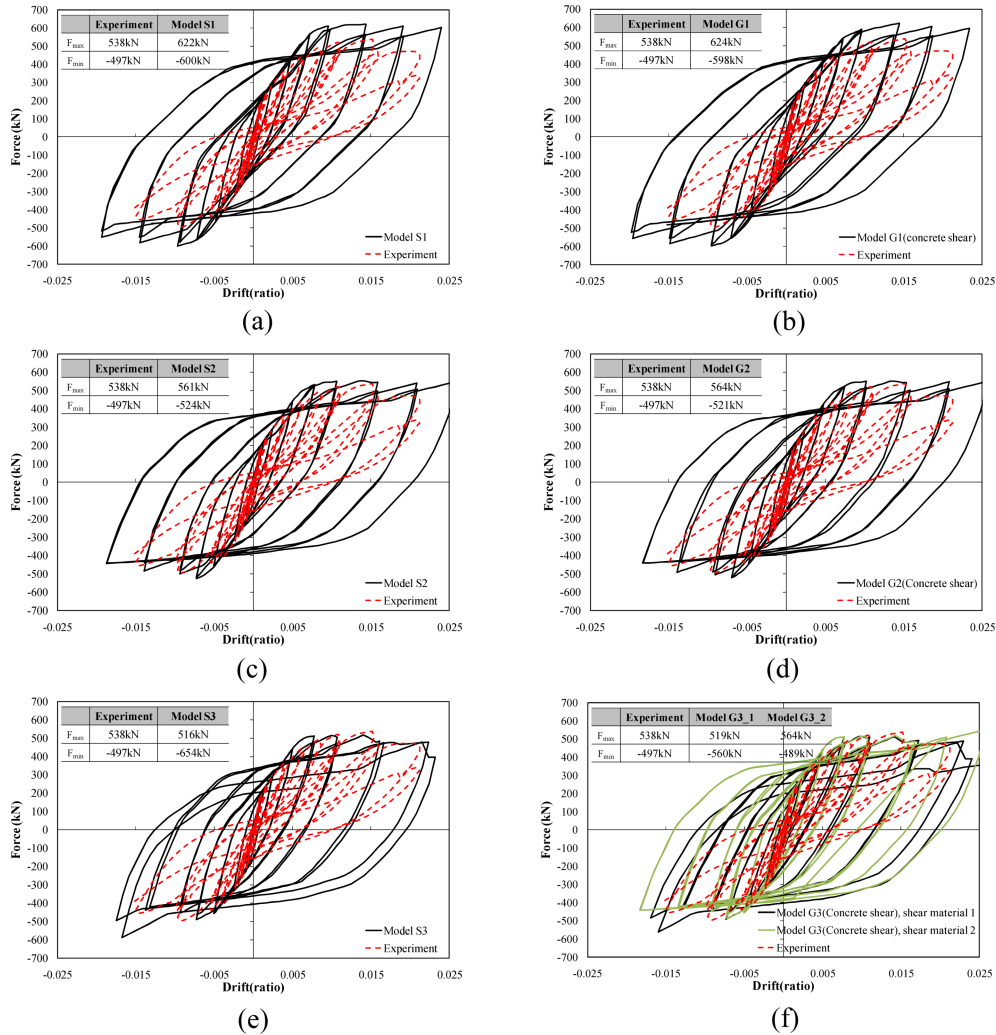


Fig. 18 Experimental and analytical relations of force-drift at top of specimen-Concrete shear: (a) Model S1(Shear Wall), (b) Model G1(General Wall/Concrete Shear), (c) Model S2(Shear Wall), (d) Model G2(General Wall/Concrete Shear), (e) Model S3(Shear Wall) and (f) Model G3(General Wall/Concrete Shear)

overall shape of the hysteretic curves of Model G1 using “General Wall/Diagonal shear” simulates that of the experiment result fairly well, being different from that of Model G1 using “General Wall/Concrete shear” (Fig. 18(b)). Also, the maximum and minimum strengths are similar to those of the experimental results.

In contrast, in Fig. 19(g) the maximum strengths of Model G2 and G3 using “General Wall/Diagonal shear” are approximately half that of the experiment result, and initial stiffness also is significantly lower than that of the experiments. The hysteresis curves of Models G2 and G3 show extreme pinching phenomena, leading to a significant reduction in energy absorption, which essentially differs from the test results.

In Figs. 19(a) and (b), Model G4, which is derived from Model G3 by dividing horizontally the

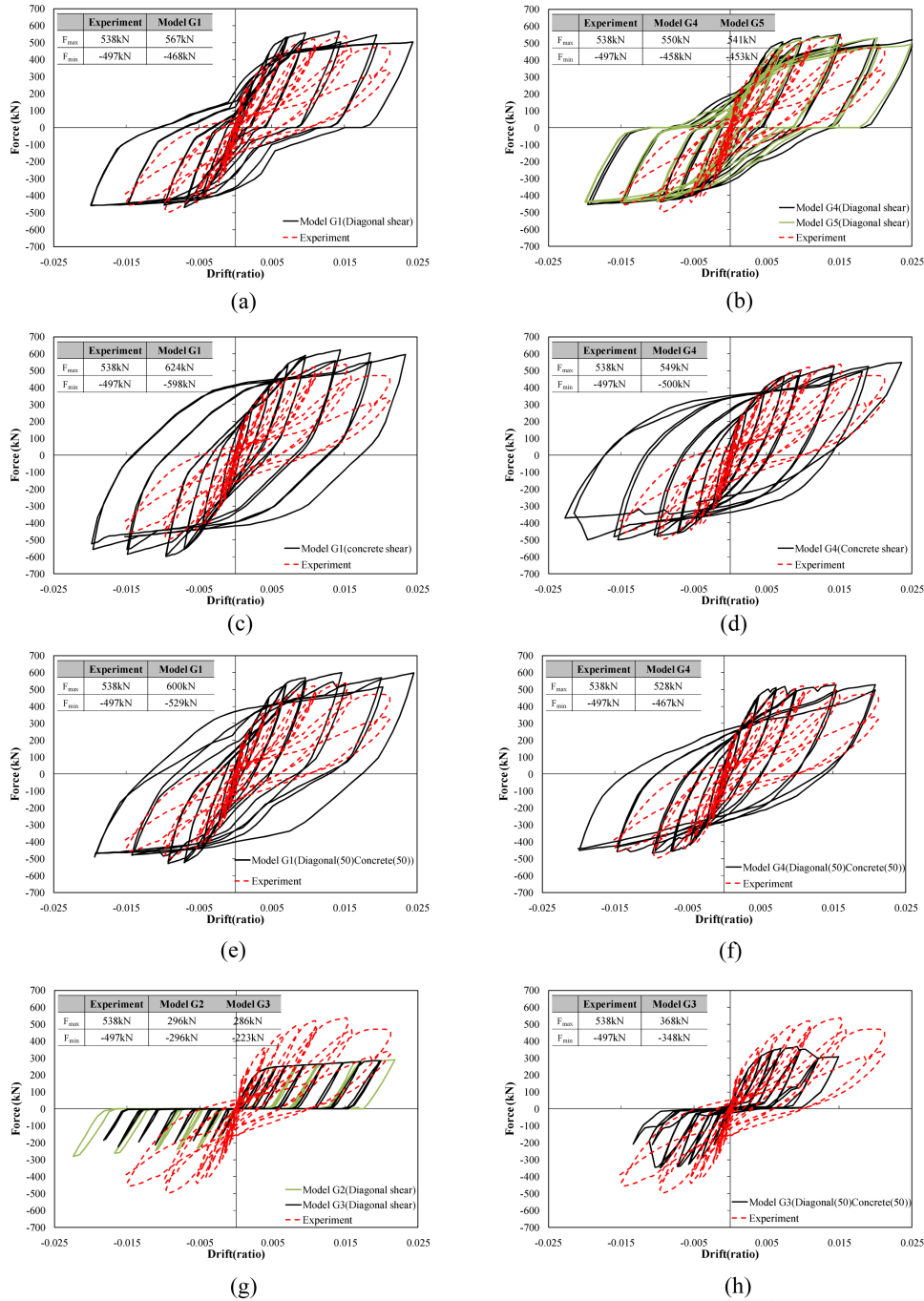


Fig. 19 Experimental and analytical relations of force-drift at top of specimen-Diagonal shear: (a) Model G1(Diagonal shear), (b) Model G4/G5(Diagonal shear), (c) Model G1(Concrete shear), (d) Model G4(Concrete Shear) (e) Model G1(Diagonal 50 Concrete 50), (f) Model G4(Diagonal 50 Concrete 50), (g) Model G2/G3 (Diagonal shear) and (h) Model G3(Diagonal 50 Concrete 50)

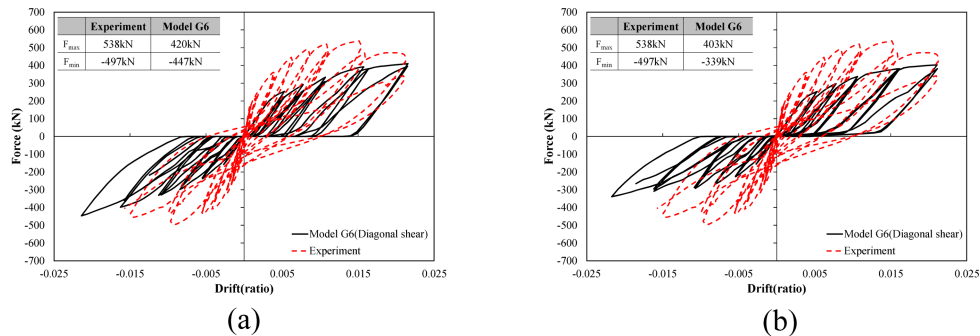


Fig. 20 Experimental and analytical relations of force-drift at top of specimen (Model G6): (a) One-element wall beam and (b) Two-element wall beam

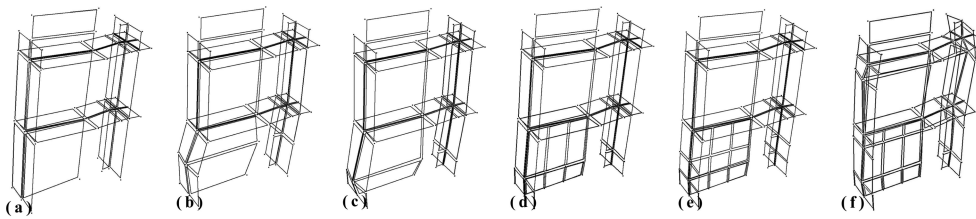


Fig. 21 Deformed shapes of models - Diagonal shear: (a) Model G1, (b) Model G2, (c) Model G3, (d) Model G4, (e) Model G5 and (f) Model G6

web-wall element in the first story into three pieces, shows better correlations in the hysteretic behaviors of the experimental result than Model G1, especially in the range from unloading to reloading. On the other hand, Model G4 using “General Wall/Concrete shear” reveals smaller energy absorption in Fig. 19(d) than other G series models using “General Wall/Concrete shear”, but, still shows significantly larger energy absorption in the reloading range than the experimental result. Nevertheless, this model improves the behavior of Model G4 (Diagonal shear) in the unloading range by reducing energy absorption due to the pinching phenomena of Model G4 (Diagonal shear) shown in Fig. 19(b).

Model G5, which is more refined than Model G4, shows almost identical hysteretic behaviors as those of Model G4 as shown in Fig. 19(b). Model G6, which replaces the coupling beam model in Model G5 by one “General Wall” element with Diagonal layer”, has shown worse correlations than Model G5, in Fig. 20(a). In Fig. 20(b), the hysteretic behavior of Model G6 with two “General Wall” elements for coupling beams has not improved the correlation.

To improve the correlations between analysis and experiment, the combined use of “Concrete shear layer” and “diagonal compression layer” stated in section 3.1.2 is attempted. One approach to a combination is to introduce 50% of “Concrete shear” and 50% of “Diagonal layer” in Model G3 and Model G4. The following can be observed in Figs. 19(f) and (h): (1) The combination of “Concrete shear” and “Diagonal shear” has improved, to a limited extent, the behavior of Model G3 with “Diagonal shear” only, but still fails to simulate the experimental results. (2) Model G4 with the combined Concrete and Diagonal shear improves greatly the behaviors of Model G4 with “Diagonal shear” only and with “Concrete shear” only, particularly by reducing the erroneous energy absorption in the unloading and reloading ranges, respectively.

Fig. 21 shows the deformed shapes of six models in the positive direction. Deformed shapes of Model *G2* and Model *G3* reveal large horizontal expansion at the boundaries between the two elements of the first-story web wall. The same phenomenon of swelling out at the belly can also be noticed in Model *G4* and Model *G5*, though the degrees of expansion are reduced. This phenomenon can be avoided by using “Shear Wall” or “General Wall” with “Concrete shear” or it can be reduced by using one “General Wall” element for one story and a finer division in the horizontal direction.

The reason why modeling approaches other than *G1*, *G4* and *G5* do not provide good predictions is now explained as follows: As the concrete cracks and the steel yields in bending behaviors, the neutral axis shifts. This means that a bending moment causes not only curvature, but also axial extension. As explained in Fig. 10 and Fig. 11, the “Diagonal compression layer” will offer no shear resistance until one of the diagonals goes into compression. Actually, this phenomenon describes roughly the pinching effect in shear resistance. However, when this “Diagonal compression layer” model is used such as in the cases of *G2* and *G3* models, only half of the total transverse reinforcement contributes to the shear resistance. Furthermore, the diagonal stirrups will usually be flexible relative to the compression, so most of the effective shear deformation is due to stretching of the stirrups rather than compression of the diagonals in shear model of “Diagonal compression layer”. Therefore, these characteristics of “Diagonal compression layer” models caused not only the swelling out at the belly, but also much lower shear strength and initial stiffness than experimental results as shown in Figs. 19(g) and (h).

4.2 Local behaviors

As mentioned previously, since the data acquisition from the instrumentation to measure flexural and shear deformation of the lower quarter portion of the first-story web wall was not successful, the upper three-quarter portion of the same wall is taken for observation on the local hysteretic behaviors hereafter. Performance-based seismic engineering (PBSE) requires the nonlinear analysis of existing or new building structures for estimation of demands and compares these demands with the capacity of corresponding critical members (FEMA 356, ASCE/SEI 41). The demands are quantified structural responses such as the maximum plastic rotations, curvatures and strains at the critical members. Therefore, it is necessary for analysis software to provide output regarding these demands. PERFORM-3D includes “Gage” elements, which are fictitious without any effect on the structural behavior, to estimate rotations and shear deformations of wall, elongations or strains.

Although the simulations of shear behavior by Model *G3* (Concrete shear) and Model *G3* (Diagonal shear) appear to significantly differ from the experimental result, those of flexural behavior are satisfactory as shown in Fig. 22(a). The simulation by Model *G3* (Diagonal layer) gives much lower shear strength and exceptionally larger inelastic deformation than the experimental results. The physical influence of the cyclic degradation parameters on the shape of the cyclic shear response (shear material) is shown in Fig. 22(b) for the model *G3* (General wall/concrete shear). Model *G3* (Concrete shear) does not simulate the pinching behavior of the experimental result, and shows different shapes of shear hysteresis in Fig. 22(b) with different energy factors (Concrete shear 1 (1.0, 0.3, 0.25, 0.2, 0.1) and Concrete shear 2 (1.0, 0.85, 0.7, 0.4, 0.3)). However, it is noted that peak deformations are identical for two models having different energy factors although the amounts of the dissipated energy differ. Energy factors with Concrete shear 2 have been adopted for all the other analyses using “Concrete shear” models.

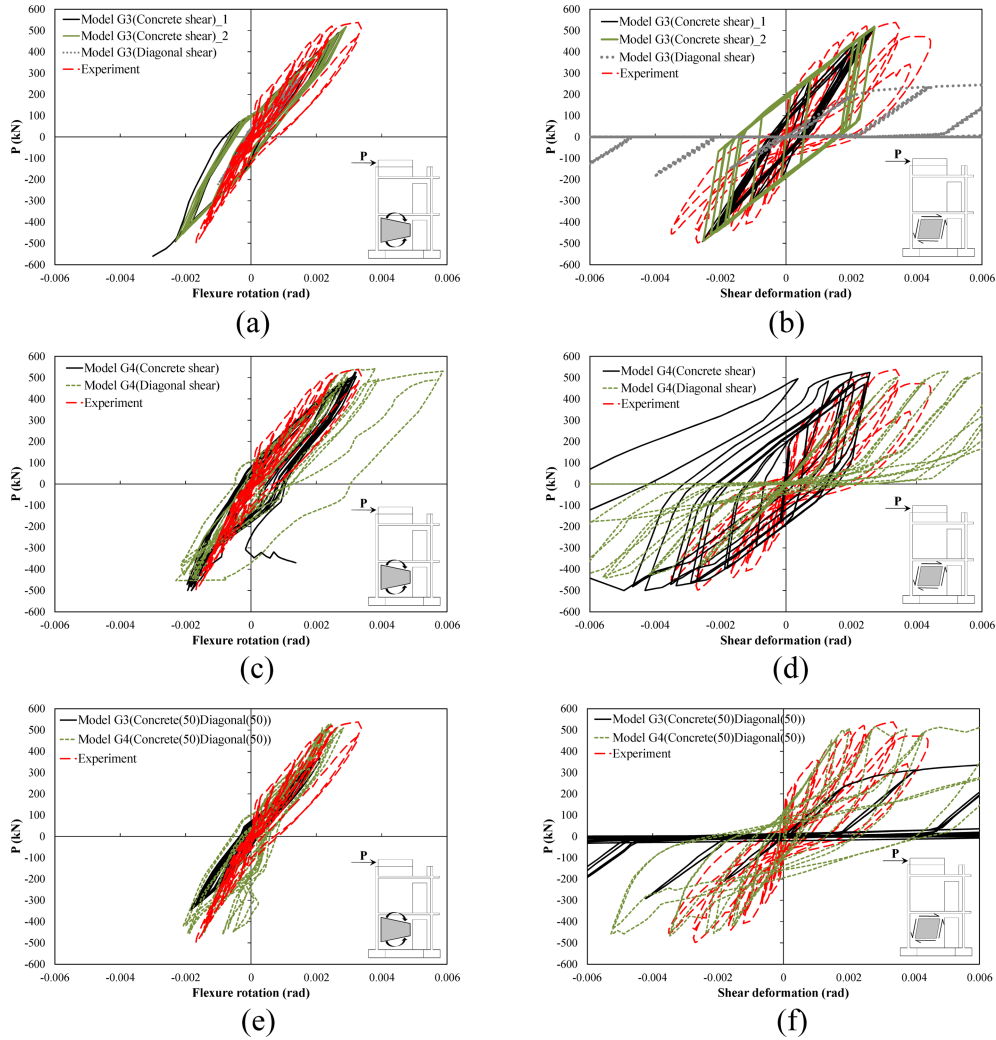


Fig. 22 Comparison of experimental and analytical relations in the upper 3/4 region of 1st-story wall: (a) Lateral force-flexural rotation, (b) Lateral force-shear deformation, (c) Lateral force-flexural rotation, (d) Lateral force-shear deformation, (e) Lateral force-flexural rotation and (f) Lateral force-shear deformation

In Figs. 22(c) and (d), Model G4 (Diagonal shear) roughly simulate flexural and shear hysteresis of the experimental results. However, the initial stiffness of shear hysteresis is greatly underestimated and relatively large plastic flexural deformations are observed in the analysis, which contradicts those in the experiment. Also, the coupling of flexural and shear yielding can be noticed both in the experiment and in the analysis as stated in the references (Orakcal and Wallace 2006, Wallace 2007). The idea of combining 50% “Concrete shear” and 50% “Diagonal shear” was attempted as shown in Figs. 22(e) and (f). This attempt was successful only for the case of G4. In the case of G4 with the combined shear models, the shape of hysteresis simulates both the envelope and pinching phenomenon with significantly improved accuracy.

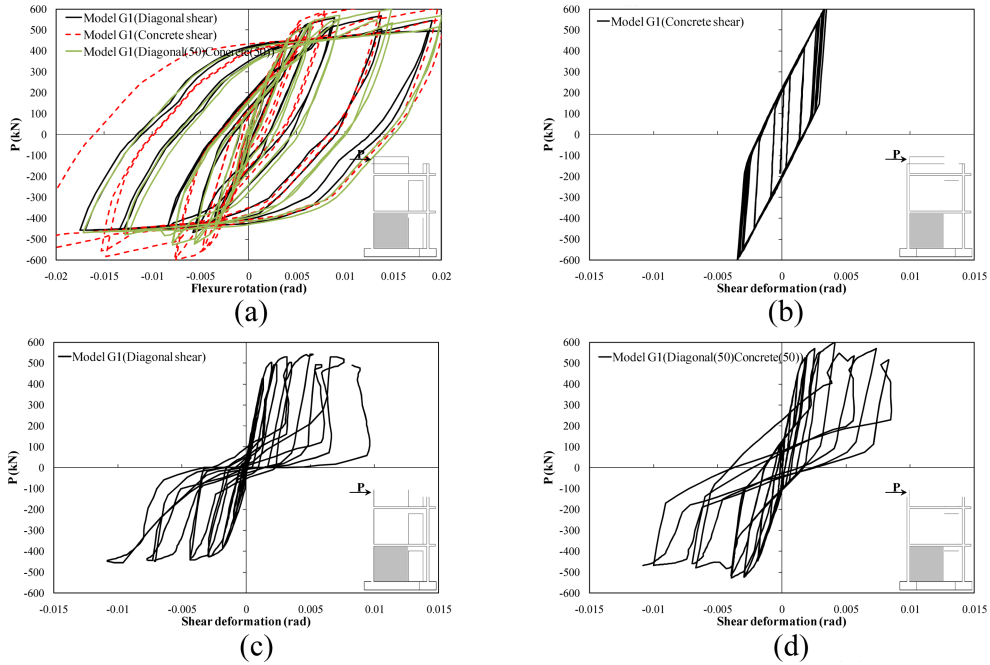


Fig. 23 Analytical relations of force at top of the specimen versus flexural and shear deformation in the 1st-story wall in Model G1: (a) Lateral force-flexural rotation, (b) Lateral force-shear deformation, (c) Lateral force-shear deformation and (d) Lateral force-shear deformation

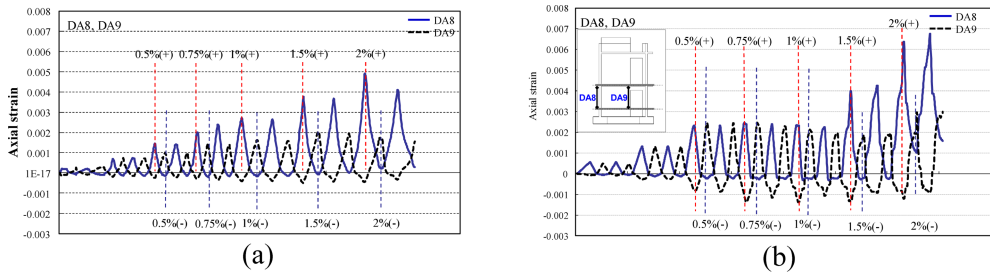


Fig. 24 Correlation of concrete strains of DA8 and DA9 (Model G4/Diagonal): (a) Experiment and (b) Analysis

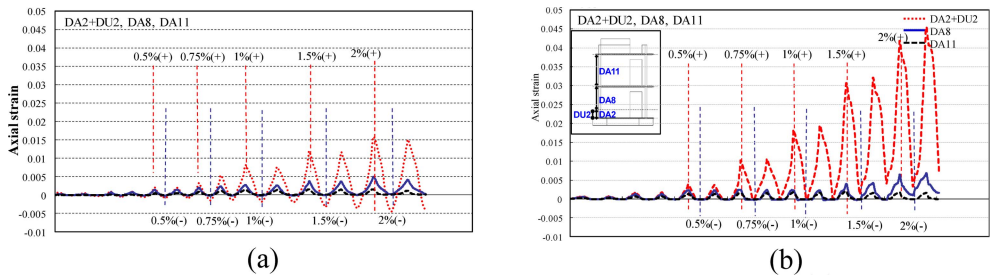


Fig. 25 Correlation of concrete strains of DA2+DU2, DA8 and DA11 (Model G4/Diagonal): (a) Experiment and (b) Analysis

Fig. 23 depicts the flexural and shear hysteresis of the first-story web wall in Model *G1* with three different shear models: (1) with 100% “Concrete shear”, the hysteresis shape is a parallelogram. (2) With 100% “Diagonal shear”, the shape reveals a high degree of pinching behavior. (3) A combination of 50% “Concrete shear” and 50% “Diagonal shear” causes the increased slope in the pinching phase, therefore alleviating the pinching.

Using “Gage” elements, the histories of elongation of *DA8* and *DA9* in the upper wall element of the first-story web wall, and those of *DU2+DA2*, *DA8* and *DA11* along the height of the specimen at the corner of the flange and web walls as shown in Fig. 3(b) are obtained for Model *G4* with “Diagonal shear” and compared with the experimental results in Figs. 24 and 25, respectively. It can be found in these figures. That the histories of deformation at specific locations may differ between experiment and analysis. Particularly, the compressive shortenings at the bottom of the wall are significantly underestimated while the tensile elongations are overestimated in the analysis. Although the histories of individual axial deformations for *DA8* and *DA9* differ somewhat between experiment and analysis, the overall relationships between the lateral force at the top of the specimen and the rotation of the upper wall element as shown in Fig. 22(c) appear to be similar. The distributions of concrete deformations along the web wall in the lower quarter region in Fig. 26 reveal again the overestimation in elongation and underestimation in shortening in the analysis.

Overestimations in the elongation side reach about 4 times those of the experimental result at the 1% drift ratio of the top displacement. Also, the distribution in analysis does not represent linear distribution implicit in the theorem of plane-sections-remain-plane. The magnitudes of elongation at the lower quarter region along the flange wall are similar between analysis and experiment as

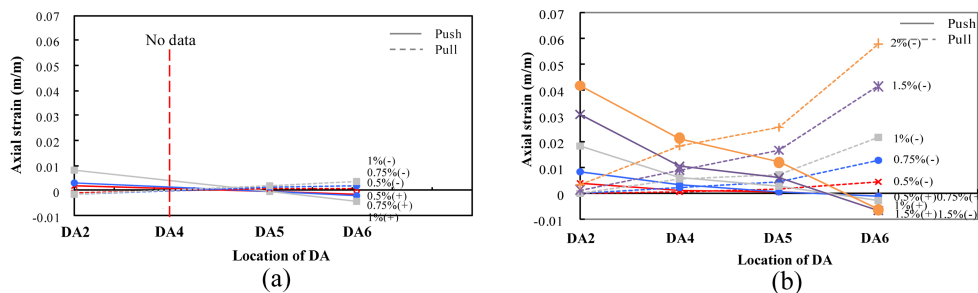


Fig. 26 Distribution of elongations in the lower quarter region of the web at 1st story (Model *G4*/Diagonal): (a) Experiment (*DA+DU*) and (b) Analysis (*DA+DU*)

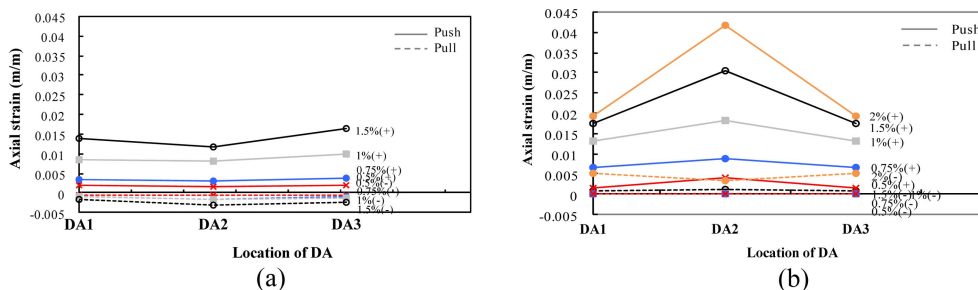


Fig. 27 Distribution of elongations in the lower quarter region of the flange at 1st story (Model *G4*/Diagonal): (a) Experiment (*DA+DU*) and (b) Analysis (*DA+DU*)

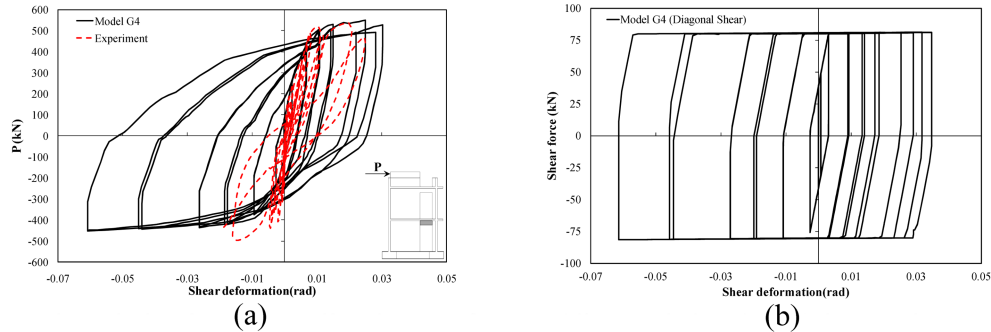


Fig. 28 Shear behavior in coupling beam of Model *G4* (diagonal shear) with beam element in Fig. 16(b) at first story: (a) Lateral force versus shear deformation and (b) Shear force versus shear deformation

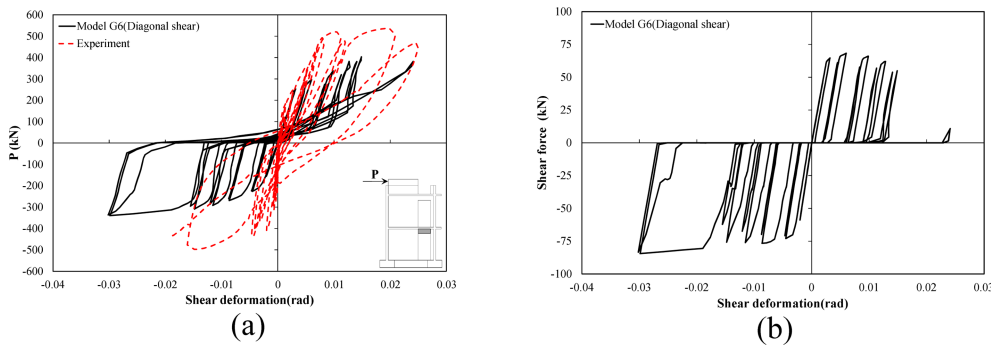


Fig. 29 Shear behavior in coupling beam of Model *G6* (diagonal shear) with two “General Wall (diagonal shear)” element: (a) Lateral force versus shear deformation and (b) Shear force versus shear deformation

shown in Fig. 27, though the distributions in analysis show larger elongation at the center than at the ends of the flange whereas those in the experiment reveal a lower elongation at the center. Finally, the hysteretic relations between the shear deformation in the coupling beams at the first story and the lateral force at the top of the specimen are shown in Fig. 28(a) with the backbone curve and hysteretic relation between the shear force and shear deformation shown in Fig. 28(b). Analysis reveals much larger inelastic deformations than the experiment in the negative direction. However, the correlations in hysteresis appear to be reasonable.

Figs. 29(a) and (b) depict the hysteresis curves of Model *G6*, which replace the beam elements in Model *G5* in Fig. 16(b) by the spandrel beams with two “General Wall” elements, between the shear deformation of the coupling beam at the first story versus the lateral force at the top of the specimen and the shear force in the coupling beam, respectively. This means that the “General Wall” element is not able to simulate reliably the shear deformation in the coupling beams.

6. Conclusions

The state of technology in performance-based seismic engineering (PBSE) has evolved to the status that the nonlinear analysis of building structures is regarded as a normal procedure for the

seismic evaluation of existing structures. Typical standard guides regarding PBSE are the FEMA 356 (FEMA 2000) and ASCE/SEI 41 (ASCE 2007) reports. For the success of PBSE, it is essential to use a reliable nonlinear analysis for the reinforced concrete wall structure. This paper attempts to find the best analytical model to simulate the global behavior by using the commercial program, PERFORM-3D, for the results of reversed cyclic lateral tests of an RC shear wall sub-assembly. The following conclusions are drawn from the research results:

- (1) “Shear Wall” and “General Wall” models, which use “Concrete shear layer”, cannot simulate the pinching phenomena due to shear and show larger amounts of energy absorption through inelastic behavior than those in the experiment.
- (2) “General Wall” models with “Diagonal layer” simulate the pinching phenomena due to shear fairly well when one element is used for one-story walls, or when several elements in both vertical and horizontal directions are used for one-story walls.
- (3) Use of “Concrete shear” induces a larger amount of inelastic energy absorption in the reloading range while use of “Diagonal layer” causes a lower initial stiffness and a larger amount of energy absorption in the unloading range of shear behavior. These disadvantages of shear models of “Concrete shear” and “Diagonal shear” can be overcome to some extent by using a combination of these two models.
- (4) Modeling a story-height wall by using two or more “General Wall” elements with “Diagonal shear” only in the vertical direction shows the phenomenon of swelling-out at the belly, leading to the erroneous simulation of shear behaviors. In practical application to tall building structures, it is recommended that one element of “General Wall” with “Diagonal shear” be used for the full height of a story.
- (5) In the plastic hinge area, concrete deformations of the analytical model generally overestimate elongation and underestimate shortening when compared with experimental results. Therefore, it is recommended that engineers be careful to estimate the demand on the concrete strains by using PERFORM-3D.
- (6) Since the use of “General Wall” elements for coupling beams has not shown reasonable analytical simulation, it is recommended that beam elements with appropriate shear and flexural plastic hinges be used.

Acknowledgments

The research presented herein was supported by the National Research Foundation of Korea through the contract No. 2011-0000373. The authors thank Dr. Graham Powell for his valuable advice at the final stage of study, which has contributed greatly to the improvement of this paper.

References

- ACI Committee 318 (2002), *Building code requirements for structural concrete and commentary (ACI 18-02/318R-02)*, American Concrete Institute, Detroit.
- ASCE/SEI 41-06 (2007), *Seismic rehabilitation of existing buildings*, American Society of Civil Engineers.
- Computers & Structures, Inc. (2006), *ETABS Plus version 9.1.1 Extended analysis of 3D building systems*, Berkeley, California.

- Computers & Structures, Inc. (2006), *PERFORM Components and elements for PERFORM 3D and PERFORM-Collapse ver 4*, CSI, Berkeley, CA.
- FEMA-356 (2000), *Prestandard and commentary for the seismic rehabilitation of buildings*, Federal Emergency Management Agency.
- Korea National Statistical Office (2010), *Population and housing census 2010*. (in Korean)
- Kwak, H.G and Kim, D.Y. (2004), "Cracking behavior of RC shear walls subject to cyclic loadings", *Comput. Concrete*, **1**(1), 77-98.
- Lee, S.H., Oh, S.H., Hwang, W.T., Park H.G., Kim, D.K. and Lee, H.S. (2010), "Static experiment for the seismic performance of a 2 story RC shear wall system", *J. Earthq. Eng. Soc. Kor. (EESK)*, **14**(6), 55-66. (in Korean)
- Martinelli, P. and Filippou, F.C. (2009), "Simulation of the shaking table test of a seven-story shear wall building", *Earthq. Eng. Struct. D.*, **38**(5), 587-607.
- McKenna, F., Fenves, G.L. and Scott, M.H. (2006), *Open system for earthquake engineering simulation*, University of California, Berkeley, CA.
- Mo, Y.L., Zhong, J. and Hsu, T.T.C. (2008), "Seismic simulation of RC wall-type structures", *Eng. Struct.*, **30**(11), 3167-3175.
- Orakcal, K. and Wallace, W.J. (2006), "Flexural modeling of reinforced concrete walls - experimental verification", *ACI Struct. J.*, **103**(2), 196-206.
- Orakcal, K., Massone, L.M. and Wallace, J.W. (2009), "Shear strength of lightly reinforced wall piers and spandrels", *ACI Struct. J.*, **106**(4), 455-465.
- Panagiotou, M., Restrepo, J.I., Conte, J.P. and Englekirk, R.E. (2006), "Seismic response of reinforced concrete wall buildings", *Proceedings of the 8th U.S. National Conference on Earthquake Engineering*, San Francisco, CA, U.S.A.
- Paulay, T. and Priestly, M.J.N. (1992), *Seismic design of reinforced concrete and masonry buildings*, John Wiley & Sons, Inc.
- PEER/ATC-72-1 (2010), *Modeling and acceptance criteria for seismic design and analysis of tall buildings*.
- Powell, G.H. (2011), *Personal communication*, Graham H. Powell, Inc. Wolfgang Road Truckee, California.
- Schotanus, M.I.J. and Maffei, J.R. (2008), "Computer modeling and effective stiffness of concrete wall buildings", *Proceedings of the International FIB Symposium on Tailor Made Concrete Structures –New Solutions for Our Society*, Amsterdam, Netherlands.
- Wallace, W.J. (2007), "Modeling issues for tall reinforced concrete core wall buildings", *Struct. Des. Tall Spec.*, **16**(5), 615-632.